SIMULATION OF HEATING AND CURRENT DRIVE SOURCES FOR SCENARIOS OF THE ITER RESEARCH PLAN

M. SCHNEIDER[1], E. LERCHE[2,3], D. VAN EESTER[3], O. HOENEN[1], T. JOHNSON[4], V. MITTERAUER[1], S.D. PINCHES[1], A.R. POLEVOI[1], E. POLI[5], M. REICH[5]
[1] ITER Organization, Route de Vinon-sur-Verdon, CS 90 046, 13067 St. Paul-lez-Durance, France
[2] LPP-ERM/KMS, Association Eurofusion-Belgian State, TEC partner, Brussels, Belgium
[3] Euratom/CCFE Fusion Association, Culham Science Centre, Abingdon, United Kingdom
[4] KTH Royal Institute of Technology, 10044 Stockholm, Sweden
[5] Max-Planck-Institut für Plasmaphysik, Garching bei München, Germany

Email: mireille.schneider@iter.org

Abstract

Predicting the impact of Heating and Current Drive (H&CD) sources is essential to evaluate the performance of ITER plasmas and to subsequently optimise the scenarios for the four stages of the ITER Research Plan. This should be done in the context of global transport calculations of complete plasma discharges. For this purpose, a dedicated workflow has been developed in the ITER Integrated Modelling and Analysis Suite (IMAS) as a modular component to be used together with transport solvers to quantify the dynamics of H&CD sources for the different phases of a plasma discharge, including possible synergetic effects between the heating sources. This paper presents the results of the combined modelling of H&CD sources for the ITER DT baseline 15 MA / 5.3 T scenario including the synergy between Neutral Beam Injection (NBI) of deuterium, fusion-born alpha particles and Ion Cyclotron Resonance Heating (ICRH) at the fundamental frequency of deuterium , showing modest synergetic effects. The results of the combined H&CD sources for an ITER 7.5 MA / 2.65 T helium plasma of the second Pre-Fusion Power Operation phase (PFPO-2) are also shown, exhibiting more significant synergetic effects between the fundamental ICRH minority hydrogen heating and NBI hydrogen beams. Finally, a study of ECH absorption for an ITER helium PFPO scenario at 7.5 MA / 2.65 T is also presented with a discussion on the edge parasitic absorption that arises under specific conditions.

1. INTRODUCTION

The Integrated Modelling & Analysis Suite (IMAS) is being developed to provide a standard framework for supporting scenario preparation and plasma operation at ITER. It relies on a fusion domain specific data model, which is use case agnostic (code and fusion device). The IMAS data model is made of a set of pre-defined Interface Data Structures (IDS), which are designed to support both simulation and experimental data [1]. The IMAS framework, composed of tools and libraries capable of manipulating IDSs, provides a high degree of modularity between physics models and physics workflows, such that a wide range of applications can be developed by reusing and extending existing software. One of the most sophisticated physics workflows developed so far in IMAS aims at modelling the Heating and Current Drive sources. The H&CD workflow developed by the ITER Organization is based upon an earlier development carried out within the European Integrated Modelling activities [2,3]. It has been written in Python for its ease of programming and portability, and its extensive use within the modelling community worldwide.

The IMAS Python H&CD workflow offers the capability to be coupled to any transport solver adapted to IMAS, which is a natural consequence of the standardised data model approach of IMAS. It can simulate the synergy between H&CD sources and provides a high degree of modularity between various H&CD models for all the heating sources available in ITER, i.e. Electron Cyclotron Heating (ECH), Ion Cyclotron Resonance Heating (ICRH), Neutral Beam Injection (NBI), and nuclear fusion reactions, thus covering all scenarios within the ITER Research Plan [4].

This paper addresses only heating synergetic effects between the various ion populations. The heating synergetic effects between RF waves, NBI ions and fusion-born alpha particles are quantified by the effect of the direct absorption of the RF waves on NBI fast ions and fusion-born alpha particles respectively, leading to a variation of the fast ion distributions compared to when the three heating sources (ICRH, NBI, nuclear reactions) are calculated independently, i.e. to when ICRH waves are absorbed on thermal populations exclusively. Synergetic effects usually lead to a heating efficiency superior to the efficiency obtained as the sum of the two heating mechanisms evaluated separately. This is due to the fact that the pre-heating from the beams or fusion reactions increases the plasma temperature making it less collisional, hence leading to higher energy fast ion distributions. As it will be shown in this paper, this is not necessarily the case. In the 2.65 T / 7.5 MA helium scenario studied in this paper, the synergetic effect leads to an off-axis RF absorption by NBI ions where the plasma is more collisional. As a result, the fast ion distributions are less energetic, leading to a reduced neutron rate production, which will be referred to as negative synergy.

As an application of the H&CD workflow, and to demonstrate its capability to simulate the synergy between the various H&CD sources, it has been applied to predict the H&CD performance for an ITER DT baseline 15 MA / 5.3 T scenario, including synergetic effects between NBI, fusion-born alpha particles and ICRH, and for an ITER helium 7.5 MA / 2.65 T scenario. To simulate these synergetic effects, the H&CD calculations require the complete solution of the fast ion distributions from NBI and fusion reactions before evaluating the Ion Cyclotron (IC) wave absorption. The algorithm of the H&CD workflow has been made universal to enable adjusting the sequence of codes for calculating each H&CD process according to the specific physics studies and phenomena under consideration. Another application described in this paper is the simulation of the ECH absorption at 7.5 MA / 2.65 T, including a study of the Electron Cyclotron Heating (ECH) and Current Drive (ECCD) efficiency with variations of the magnetic field and of the wave polarization. The availability of H&CD systems for each phase of the four-stage approach of the ITER Research Plan is described in Section 2. The details of the H&CD workflow implementation are described in Section 3. Results of ICRH synergetic effects with fast ions are presented in Section 4 for the ITER DT 15 MA / 5.3T baseline scenario, and Section 5 for an ITER helium 7.5 MA / 2.65T PFPO scenario. The study of ECH absorption for an ITER helium 7.5 MA / 2.65 T scenario is shown in Section 6. Finally, conclusions are drawn in Section 7.

2. THE H&CD SYSTEMS IN THE ITER RESEARCH PLAN

Within its staged approach, the ITER Research Plan consists of four distinct phases:

— **First Plasma** will consist of hydrogen. At the beginning of ITER operation, only one Upper Launcher of the EC system will be operational. It will be associated with 7-8 gyrotrons at a frequency of 170 GHz, leading to a total injected power of up to 5.8-6.7 MW into the plasma.

— **The 1st Pre-Fusion Power Operation phase (PFPO-1)** will consist of hydrogen and/or helium plasmas (to avoid activation of the machine by fusion-born neutrons). For this phase, the full EC system will be operational consisting of an equatorial launcher (with two co- and one counter-current mirrors) and four upper launchers (each with two co-current mirrors), injecting 170 GHz waves from twenty-four gyrotrons, providing up to 20 MW inside the plasma, with an additional 10 MW power upgrade being analysed for technical implementation.

— **The 2nd Pre-Fusion Power Operation phase (PFPO-2)** also consists of hydrogen and/or helium plasmas. For this phase, all the H&CD auxiliary systems will be operational:

- Five launchers of the EC system, injecting 170 GHz waves with a power of up to 20 (+10) MW as in PFPO-1;
- Two antennas of the IC system, injecting waves of tuneable frequency in the range [40-55] MHz with a power of up to 20 MW coupled to the plasma;
- Two individually controlled NBI boxes injecting hydrogen beams with an energy of up to 870 keV and a power of up to 33 MW (16.5 MW per injection box).

— **The Fusion Power Operation phase (FPO)** which corresponds to when the tokamak will become activated. The plasmas will be formed from deuterium and tritium. For this phase, only the NBI system will be modified, injecting deuterium beams with an energy of up to 1 MeV giving a power of up to 33 MW. For the DT phase, an additional H&CD source is foreseen coming from the fusion reactions generating alpha particles of 3.5 MeV energy with a power of ~100 MW for a typical baseline ITER DT scenario at 15 MA and 5.3T with Q = 10.

The combination of all these H&CD sources creates various populations of fast ion distributions which can influence the efficiency of the IC wave absorption and the corresponding deposition profiles. In the ITER PFPO-2 and FPO phases, a synergetic effect between the NBI-induced fast ions and the ICRH waves is expected to take place. The magnitude of this effect will depend on the chosen heating schemes, namely those which have a cyclotron resonance with beam ions inside the plasma [5,6]. In the FPO phase, fusion-born alpha particles may also impact the overall ICRH wave absorption and the concomitant power transfer to the electrons and ions of the plasma bulk. These physics aspects will be discussed in this paper.

3. THE IMAS PYTHON H&CD WORKFLOW

The first version of the IMAS Python H&CD workflow has been developed based upon the efforts carried out within the European Integrated Modelling activities but has later been generalised in order to offer a flexible

choice of code sequences to the modellers, and to enable specific physics studies such as the synergetic effects between various H&CD sources described here. The IMAS H&CD workflow has been designed to be used as a sub-component of a High Fidelity Plasma Simulator, in a modular way, i.e. as an interchangeable workflow component. Fig. 1 schematizes the use of the H&CD workflow as part of the actuator component of a self-consistent resolution between transport equations and free-boundary equilibrium. Ultimately, the actuator component will be embedded within a control loop ensuring a proper actuator response from the synthetic diagnostic measurements, for which another workflow is under development. The H&CD workflow has recently been integrated within the JINTRAC transport solver [7].

To ensure modularity, i.e. to facilitate their assembly and interchangeability, workflows have to follow a minimum set of rules: they have to exclusively exchange IDSs with an optional parameter file for each sub-workflow or physics actor. Several IMAS workflows are being developed under this concept, e.g. the MHD workflow [8] and an upcoming workflow for synthetic diagnostics.

It is essential to also offer modularity for workflow components, to enable choosing among a selection of models for each physics process. This is facilitated when the physics models themselves are adapted to IMAS, which implies that they exchange IDSs exclusively, with an optional code parameter file (one for each physics component), such that physics models that share the same IDS signature can be swapped in a straightforward manner. The list of H&CD codes currently available in the IMAS H&CD workflow is provided in Table 1.

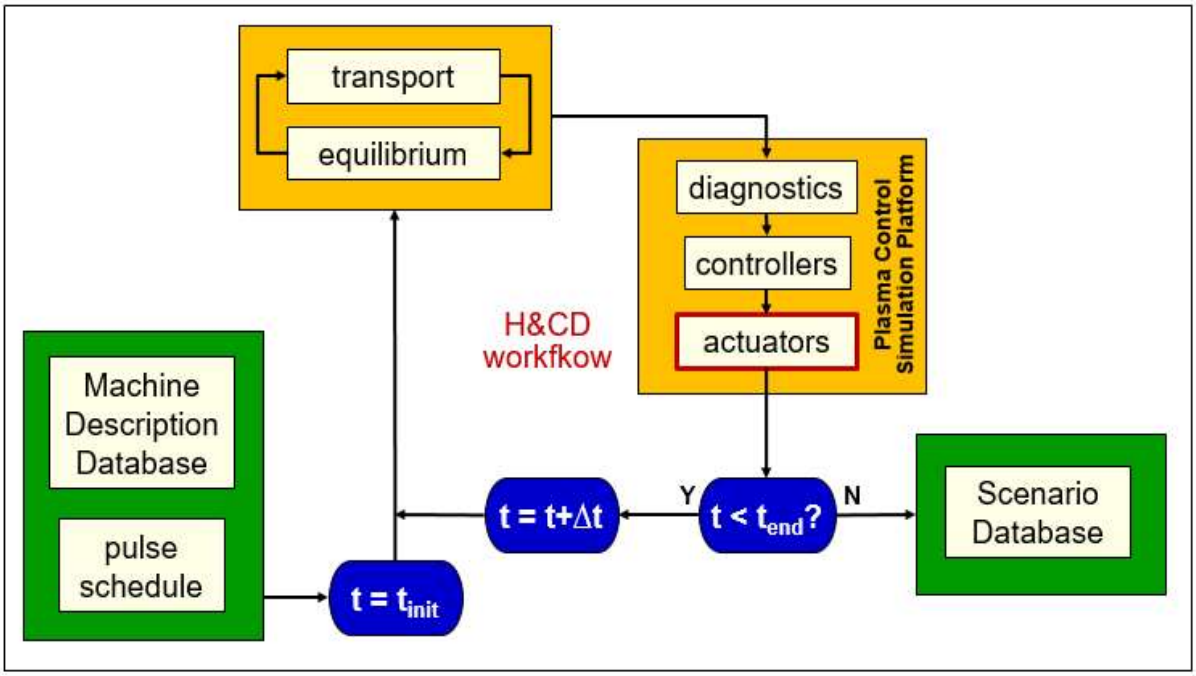

FIG. 1. Diagram of the use of the H&CD workflow in a High Fidelity Plasma Simulator, with input data received from a pre-programmed Pulse Schedule containing the reference waveforms and from the Machine Description database (containing the geometry of the various plant systems). Output is written to a scenario database.

TABLE 1. List of H&CD codes currently available in the IMAS H&CD workflow.

H&CD sources	**ECH**	**ICRH**	**NBI**	**Nuclear Reactions**
Wave or particle source	GENRAY [9] GRAY [10] GRAYSCALE [11] TORBEAM [12]	CYRANO [13] LION [14] PION [15] TOMCAT [16]	BBNBI [21] NEMO [22]	AFSI [24] SPOT (α)
Fokker-Planck calculation		ASCOT [17] FOPLA [18] PION SPOT [19]	ASCOT FOPLA RISK [23] SPOT	ASCOT FOPLA SPOT

The simulation of an H&CD process usually requires the modelling of a source (a wave or a particle source through beam deposition or nuclear reactions) associated with a Fokker-Planck calculation, to solve the dynamics of the resulting electron or ion populations due to the slowing-down of the fast particles. For ECH, since no Fokker-Planck code is currently available in IMAS, wave absorption and current drive are evaluated through linear models which are part of each EC wave solver.

Each H&CD model produces one or more output IDSs that are propagated to the rest of the workflow. The output IDSs for H&CD calculations are *waves*, *distribution_sources* and *distributions*. When several codes have the same IDS output (e.g. *waves* filled by both EC and IC wave solvers), they are merged together via merger components, to propagate only one instance of each IDS within the workflow, to keep the IDS bundle simple. At the end of each time iteration of the workflow, the sources are combined together to deliver a unique *core_sources* IDS to be used in the transport equations of the High Fidelity Plasma Simulator. One can also optionally fill the fast ion contributions of the *core_profiles* IDS to also be used in transport calculations. These two operations are performed by two dedicated actors called 'hcd2core_sources' and 'hcd2core_profiles'. All these steps are illustrated in Fig. 2. By default, the H&CD workflow first calculates all the sources (i.e. the wave, NBI and nuclear sources), then it solves the Fokker-Planck equations for each of these sources, and next merges them all together before filling the core sources and profiles for the solution of the transport equations. This default algorithm is illustrated in Fig. 2.a. However, to calculate the synergetic effects between NBI, nuclear reactions and ICRH, the IC wave solver needs to receive the complete solution of the fast ion distributions, which means that the distributions of ions originated from NBI and nuclear sources have to be calculated through Fokker-Planck calculations prior to the evaluation of the wave absorption which includes an iterative loop to converge to a consistent solution between the wave absorption and the fast ion distributions. This algorithm is illustrated in Fig. 2.b. The H&CD workflow allows the modeller to customize and refine the specific algorithm adopted according to the physics processes to be simulated: the sequence of codes can be stored in pre-defined lists within the workflow configuration (at the moment two pre-defined lists exists, corresponding to the sequences depicted in Fig. 2.a and 2.b). New lists can be defined for new specific studies. The workflow automatically decides if mergers are needed and when to call them. If a specific H&CD process is not requested by the modeller, it is simply removed from the predefined sequence.

For example, the sequence for NBI + nuclear reactions + ICRH synergy is specified in the input configuration (where all the possible processes and calculations of the workflow are systematically defined): [ec_wave_solver, nbi_source, nbi_fp, nuclear_source, nuclear_fp, ic_wave_solver, ic_wave_fp, fill_core_sources, fill_core_profiles]. For the study of the ITER DT 15MA / 5.3T baseline scenario presented in this paper, ECRH was not activated. The filling of the *core_sources* IDS was activated but not that of *core_profiles*. Hence, the resulting sequence was automatically adjusted by the workflow and became: [nbi_source, nbi_fp, nuclear_source, merge_distribution_sources, nuclear_fp, merge_distributions, ic_wave_solver, ic_wave_fp, merge_distributions, fill_core_sources]. Note that the 'merge_distributions' module is called twice: first to merge the distributions from NBI ions and alpha particles, before the IC wave calculation, and second to merge the distributions from IC-accelerated ions (from thermal plasma) with those from NBI and alpha particles. At the end of each time iteration of the workflow, the fully merged *distributions* IDS is fed into the 'hcd2core_sources' module, along with the merged *distributions_sources* IDS from NBI and nuclear reactions, and the merged *waves* IDS from EC and IC waves.

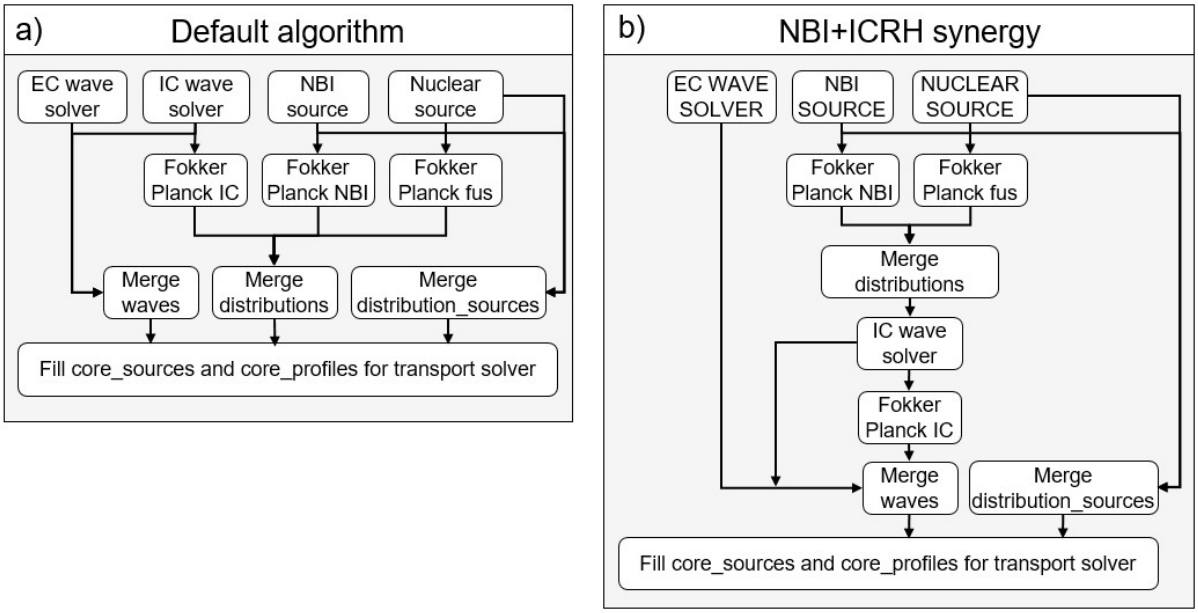

FIG. 2. H&CD workflow algorithms. (a): default algorithm for standard H&CD modelling; (b): algorithm to be used when synergy between NBI ions, fusion-born ions and IC waves has to be evaluated.

To facilitate the workflow configuration and its standalone execution outside a transport solver on existing scenarios, a GUI has been developed, from which each process can be activated or deactivated and specific models can be selected. The code parameters for the workflow configuration and its components are also directly accessible from the GUI. An example of GUI configuration is displayed in Fig. 3. So far, synergy has been demonstrated only with the FOPLA code for IC Fokker-Planck calculation (PION is also able to simulate this synergy but it has not been tested in the workflow yet). Hence, to facilitate the configuration, the workflow automatically selects the synergy algorithm when the FOPLA code is selected. Otherwise, the default algorithm is used.

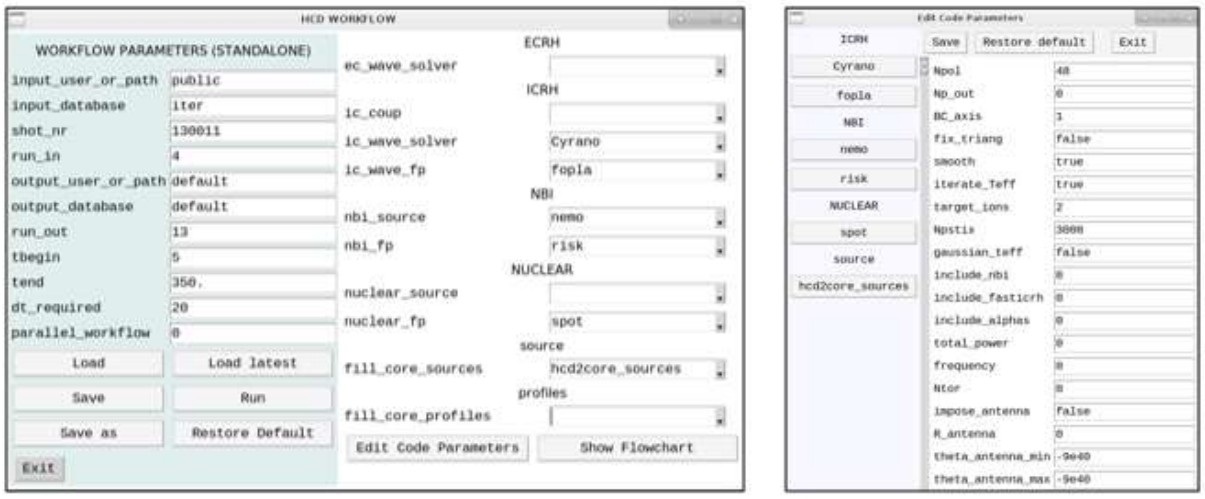

FIG. 3. Graphical interface of the H&CD workflow. Left figure: Main GUI where the time loop of the H&CD calculation can be configured for an existing scenario of the IMAS database and H&CD processes and models can be selected. Right figure: GUI to edit code parameters for each selected H&CD model.

4. SYNERGY BETWEEN NBI, FUSION ALPHAS AND ICRH FOR AN ITER DT BASELINE SCENARIO

The current study focuses on the effect of NBI and fusion-born alpha particles on IC absorption and heating. To study this effect, the NBI modelling is carried out by the NEMO beam deposition code associated with the RISK ion Fokker-Planck code. The fusion-born alpha particles are simulated by the SPOT orbit following Monte Carlo

code, the IC wave absorption of all the plasma species is computed by the CYRANO code and the collisional power transfer from the IC-accelerated (thermal, NBI and fusion-born alpha particles) ions is simulated by the FOPLA 1D Fokker-Planck solver. The ECH calculation is not activated in this modelling since the purpose is to analyse the interplay between the ions heated by ICRH, the ions coming from NBI and from nuclear reactions. ECH is already taken into account in the modelling since the input scenario was computed including 20 MW of ECH in the determination of the plasma properties.

The simplified steady-state form of the 1D velocity-dependent Fokker-Plank equations used in the FOPLA code is expressed as follows:

$$\frac{1}{v^2}\frac{\partial}{\partial v}\left[v^2\left(D\frac{\partial F_0}{\partial v}+BF_0\right)\right]+S-\frac{F_0}{\tau_p}=0$$

where F_0 is the 1D ion distribution, v is the ion velocity, $D=D_{RF}+D_{vv,coll}$, with $D_{RF}=K_{RF}\left|J_{N-1}+\frac{E_-}{E_+}J_{N+1}+J_N\frac{E_\parallel}{E_+}\right|^2$ is the quasilinear operator for the interaction between the RF waves and the ions. In this operator, E_+ and E_- are the wave RF electric field polarisation components rotating in the sense of the ions and electrons respectively, and $E_\parallel$ is the parallel electric field. J_N are Bessel functions of order N with argument proportional to the ion velocity, and S is the source term which consists of suprathermal ions from neutral beam injection and nuclear reactions when synergetic effects between RF waves and these two populations are calculated. The coefficient $B=B_{coll}+B_{loss}$, consists of $B_{coll}=-F_{v,coll}$ which is a coefficient of the collision operator, and $B_{loss}=\frac{v}{2}\left(\frac{1}{\tau_E}-\frac{1}{\tau_P}\right)$ which is the loss term introduced to achieve a steady-state solution of the Fokker-Planck equation – to compensate the source term – where τ_E and τ_P are the energy and particle loss times respectively. $D_{vv,coll}$ and $F_{v,coll}$ are coefficients of the collision operator for which the complete expressions can be found in [D. Van Eester et al, EFTC conf. (2019), accepted for publication in J. Plasma Phys.]. For a given ion species and given magnetic surface, K_{RF} is adjusted to ensure that the RF power density corresponding to the distribution obtained solving the Fokker-Planck equation is equal to the externally imposed RF power density. This Fokker-Planck equation is time-independent and neglects pitch angle effects and radial diffusion, to ensure a reasonably fast computation time, which is an essential criteria in integrated modelling frameworks.

The modelling results of the H&CD workflow are presented for an ITER DT baseline scenario at 15MA/5.3T, computed with the METIS transport solver [25], available within the IMAS scenario database [26]. The scenario is displayed in Fig. 4.

For this scenario, 33 MW of NBI and 10 MW of ICRH are applied. To estimate the potential synergetic effect between ICRH and fast ions (from NBI and DT fusion reactions), the IC frequency is tuned so that the fundamental D resonance is centrally located within the plasma, i.e. to 40 MHz. At this frequency, the fundamental ^{9}Be resonance is slightly off-axis on the High Field Side. Note that this scheme is not the reference heating scheme for ITER DT baseline scenarios, which is fundamental ^{3}He heating associated with 2nd harmonic T heating, for which resonances are central at a wave frequency of 53 MHz. Here the fundamental D heating has been chosen instead in order to illustrate the synergetic interaction between the NBI deuterium beams and the ICRH fundamental D heating scheme. This scenario also offers a considerable potential for RF-enhanced neutron yield, since the bulk D ions are directly accelerated by fundamental ICRH to energies that are optimal for DT fusion reactions [27,28].

To isolate the various physics processes, it is necessary to first study the wave absorption and the resulting collisional power when NBI ions and alpha particles are not included in the ICRH calculation. The results are shown in Fig. 5. As can be seen, the wave is absorbed dominantly on deuterium ions (centrally) and electrons, with also a moderate off-axis absorption on ^{9}Be. The absorbed power is then transferred through collisions to the thermal ions (dominantly D but also T) and electrons, resulting in a dominant heating in the core.

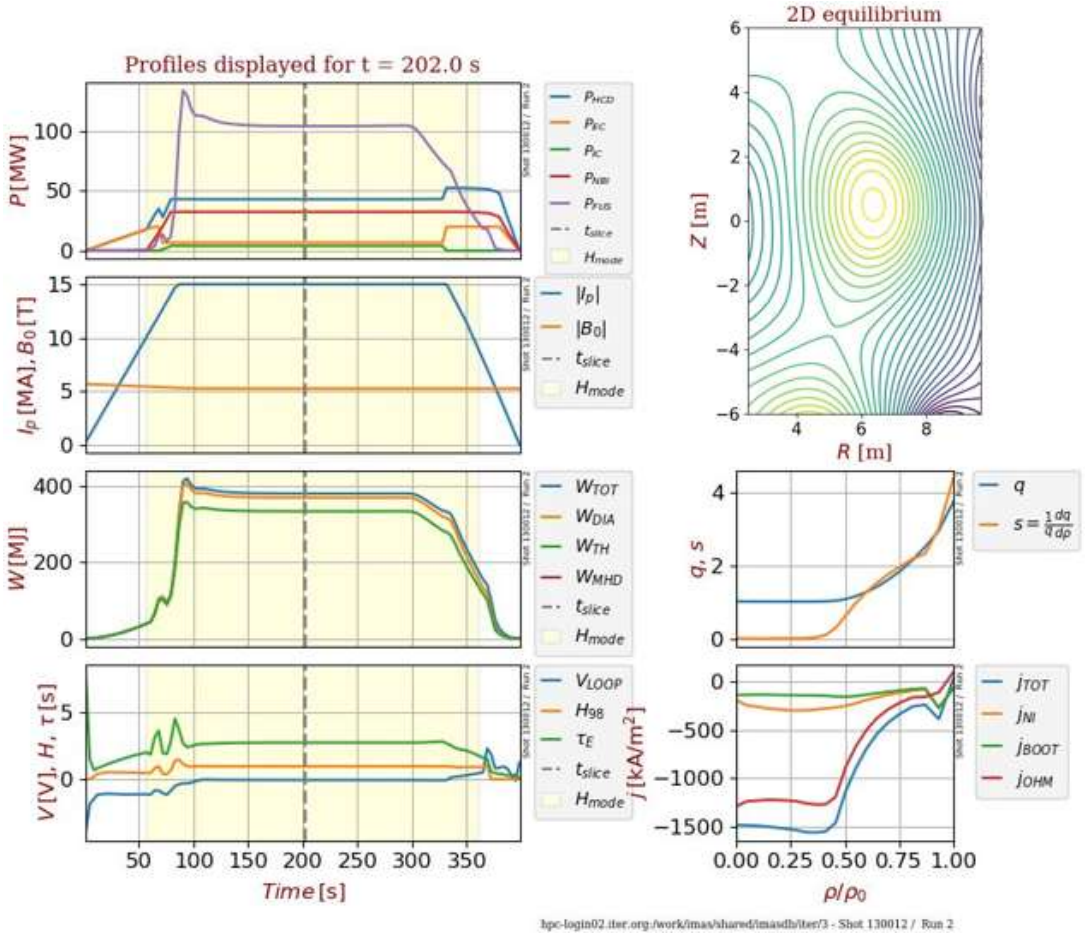

FIG. 4. ITER DT 15MA/5.3T baseline scenario computed by METIS. The yellow region represents the period when H-mode is achieved. The first figure on the left shows the power waveforms. The plasma current and magnetic field are displayed in the figure underneath. The next one displays the energy contents, and the bottom one shows the loop voltage, confinement factor and confinement time. On the right side, the 2D equilibrium, safety factor, shear and current profiles are displayed for the selected time slice.

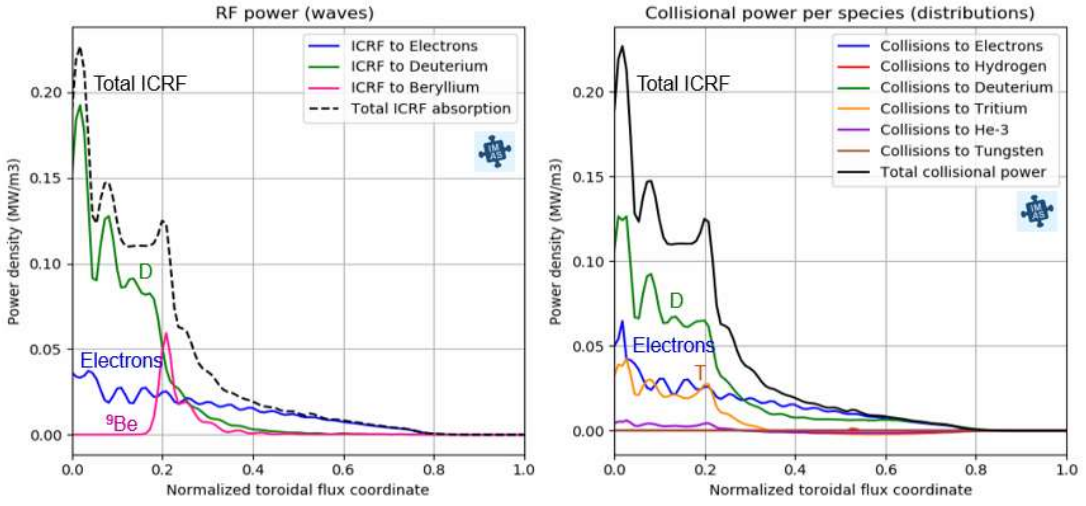

FIG. 5. ICRH absorption and collisional power transfer for the ITER DT baseline 15MA/5.3T scenario, in the ICRH only case. Left figure: IC wave absorption computed by CYRANO. Right figure: resulting collisional power to electrons and ions computed by FOPLA.

Before adding the contribution from NBI and fusion-born alpha particles, it is essential to verify that FOPLA provides a good description of the NBI and alpha distributions. For each magnetic surface considered, FOPLA calculates a 1D distribution for the NBI ions and alpha particles based on their source rates, source energies and particle densities given by NEMO/RISK and SPOT. Fig. 6 shows the comparison of the surface-averaged NBI

collisional power density between RISK and FOPLA (top figures) and of the alpha collisional power density between SPOT and FOPLA (bottom figures). As can be seen, there is a good agreement in both cases, confirming that FOPLA provides a sufficiently accurate model of the NBI and alpha particle collisional dynamics, despite its 1D representation of the fast ion distribution functions.

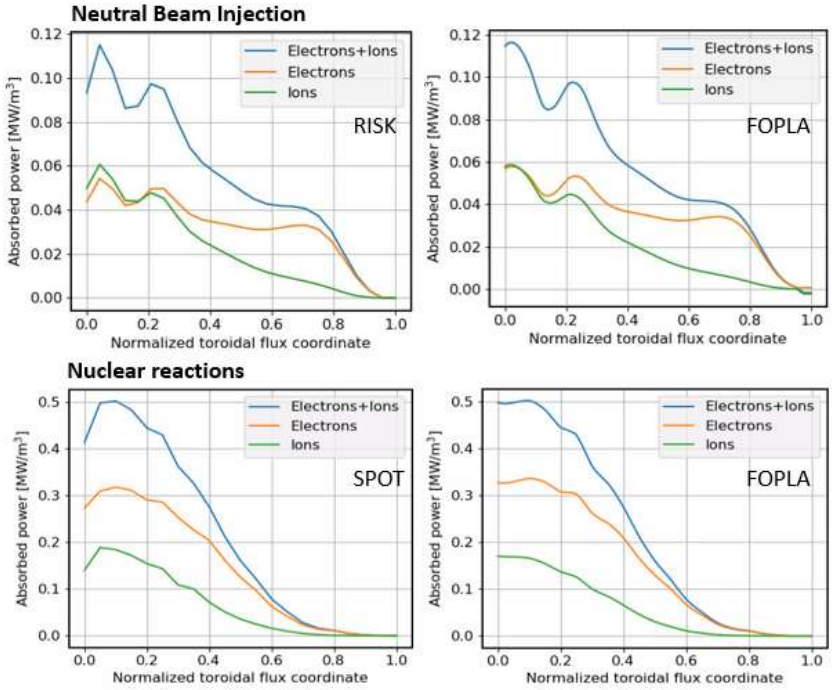

FIG. 6. Top figures: Comparison of NBI 1D collisional power density between RISK and FOPLA; bottom figure: comparison of alpha 1D collisional power density between SPOT and FOPLA.

Finally, adding the contributions from NBI and fusion-born alpha particles, the overall IC absorption and collisional power transfers are displayed in Fig. 7. As can be seen, the FOPLA input power densities (left figure) are dominated by the alpha particle collisional power density, which corresponds to a power of 96 MW. Note that the alpha fusion power evaluated by the SPOT and FOPLA Fokker-Planck codes differs from the original one calculated by METIS and shown in Fig. 4, because METIS uses a simple analytical model for calculating the alpha particle source. The NBI collisional power density is also significant (with a total of 33 MW). The IC absorption (10 MW) displays a dominant D absorption with very modest RF absorption on NBI ions and fusion-born alpha particles, showing that synergetic effects are weak for this scenario. This is partly explained by the small fraction of NBI and alpha particles present in the plasma but particularly because of their large Doppler shift in the MeV energy range, which considerably spreads the IC absorption of the fast ions to regions where the RF field polarization is not favourable in a 50:50 DT plasma. The resulting collisional power (right figure) shows a dominant electron heating, which was to be expected due to the dominant alpha power density. Combining NBI, alpha heating and ICRH results in significant core ion heating of ~40%.

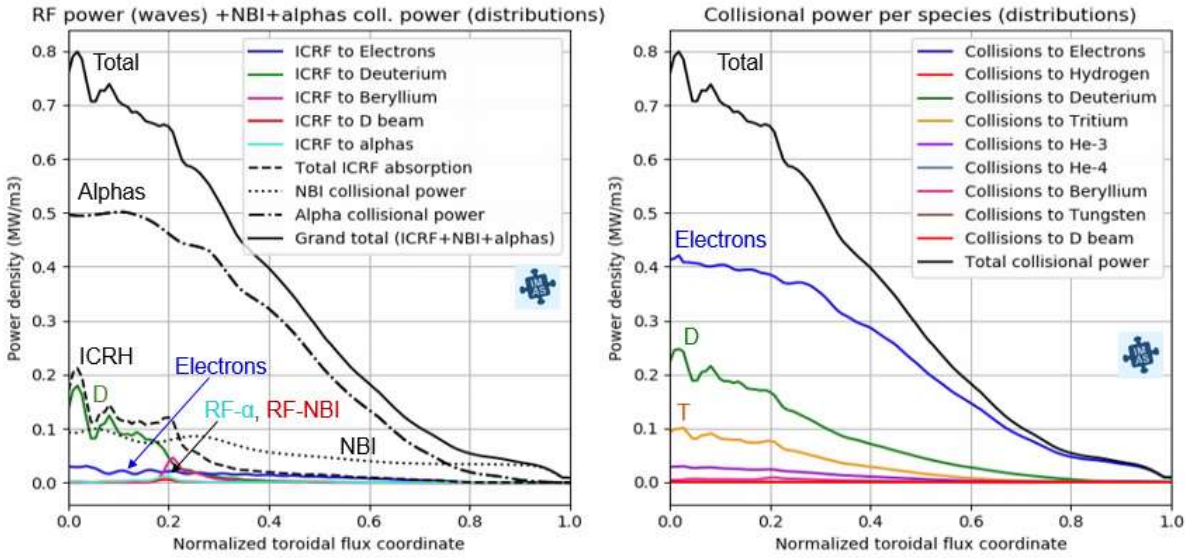

FIG. 7. ICRH absorption and collisional power transfer for the ITER DT baseline 15MA/5.3T scenario, including NBI, alpha particles and ICRH all together. Left figure: IC wave absorption computed by CYRANO along with NBI and alpha collisional power densities computed by NEMO-RISK and SPOT respectively. Right figure: Resulting total collisional power computed by FOPLA.

5. SYNERGY BETWEEN NBI AND ICRH FOR AN ITER HELIUM PFPO SCENARIO

The synergetic effect between NBI and ICRH is further studied for a PFPO-2 helium scenario at 7.5MA / 2.65T. Given that the NBI system injects 870 keV hydrogen beams in the PFPO phases, the RF frequency is tuned for fundamental H minority heating at 2.65 T, corresponding to a frequency of 43 MHz.

For this study, a scenario simulated by the JINTRAC transport solver has been selected from the IMAS scenario database, corresponding to an H-mode helium plasma with a hydrogen concentration of 10%. The kinetic profiles at the flat-top of this scenario are displayed in Fig. 8. The original H&CD configuration for this scenario was with 33 MW of NBI and 20 MW of ECH. It has been modified for the purpose of this study to 33 MW of NBI combined with 20 MW of ICRH. In addition, 1% of ^{9}Be concentration has been added in order to evaluate the neutron rates coming from ^{9}Be-p reactions.

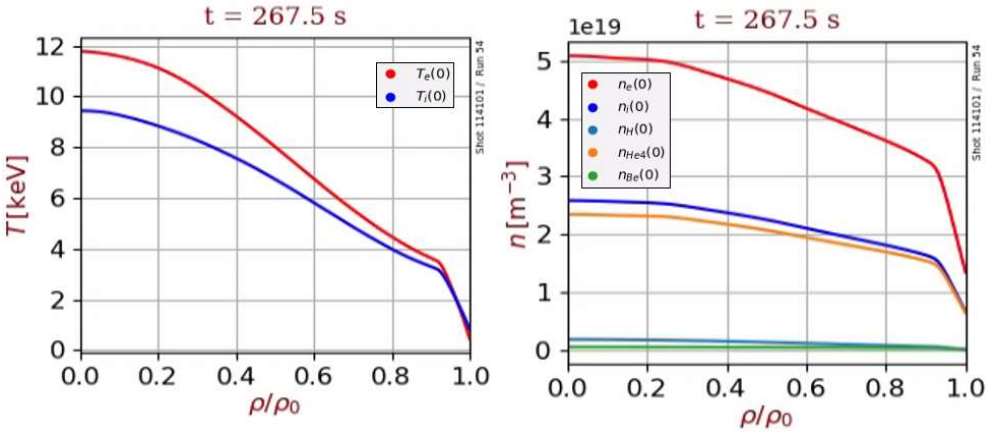

FIG. 8. Temperature and density profiles at the flat-top of a JINTRAC H-mode scenario at 7.5 MA / 2.65 T in helium.

For this modelling, the NBI distribution functions have again been simulated with NEMO/RISK, and the IC wave and Fokker-Planck calculations have been simulated with CYRANO and FOPLA respectively. The resulting RF absorbed power density profiles and the concomitant collisional power transferred to the plasma bulk have been compared between (1) simulating the ICRH and NBI sources independently and (2) accounting for the NBI+ICRH synergy. The results are presented in Fig. 9. As can be seen, the ICRF absorption on H beams starts far off-axis at $\rho/\rho_0 \sim 0.8$ (due to the large Doppler shift) and extends up to close to the centre, where the cold IC resonance is located. It results in a reduction of the RF power absorbed by the initially thermal hydrogen minority ions in the

centre. The far off-axis region where the RF power is absorbed by H beams is more collisional, due to a significantly lower local slowing down time, as shown in Fig. 10. *The slowing down is here calculated using the simplified expression from [29],* $t_s = 6.27 \cdot 10^8 \frac{A(kT_e)^{3/2}}{Z^2 n_e \log\Lambda}$ *where A and Z are the mass and charge number of the test particle,* T_e *is the electron temperature in eV,* n_e *is the electron density in cm*$^{-3}$*, and* $\log\Lambda$ *is the Coulomb algorithm. This is the characteristic time needed for a test ion to transfer its energy to the bulk plasma via collisions.* This effect associated with the relatively modest RF power densities in this region results into a globally less energetic fast hydrogen distribution and higher power transfer to the bulk ions. This is illustrated in Fig. 11 which shows the energy distributions of H beams, thermal and IC-accelerated H ions, with and without accounting for the synergetic effects between NBI and ICRH. The energy distribution of the H beam is peaked at its birth energy of 870 keV and as can be seen, the IC acceleration moderately increases its energy up to around 1.2 MeV. This is explained by the relatively low ICRF power densities associated to the H beam ions and by the fact that fundamental IC heating dominantly heats thermal species, due to the dominance of the zeroth-order Bessel function J_0 (i.e. $J_{N-1}$for fundamental heating, i.e. $N = 1$), which is maximum at a perpendicular particle velocity of zero, in the quasi-linear operator for the interaction between the IC waves and the ion populations. In contrast, the initially thermal hydrogen minority distribution is strongly heated with ICRH to energies up to around 5 MeV (first zero of the Bessel function J_0), as expected from fundamental minority heating. More interestingly, the comparison of IC-accelerated H distributions with and without synergetic effects shows that, in the presence of NBI+ICRH synergy, the number of hydrogen ions at low energy (typically below 100 keV) slightly increases, while the number of hydrogen ions at energies in the MeV-range is significantly lower than without synergy, which is explained by the highest collisionality where the IC power is absorbed by H beams, as explained above.

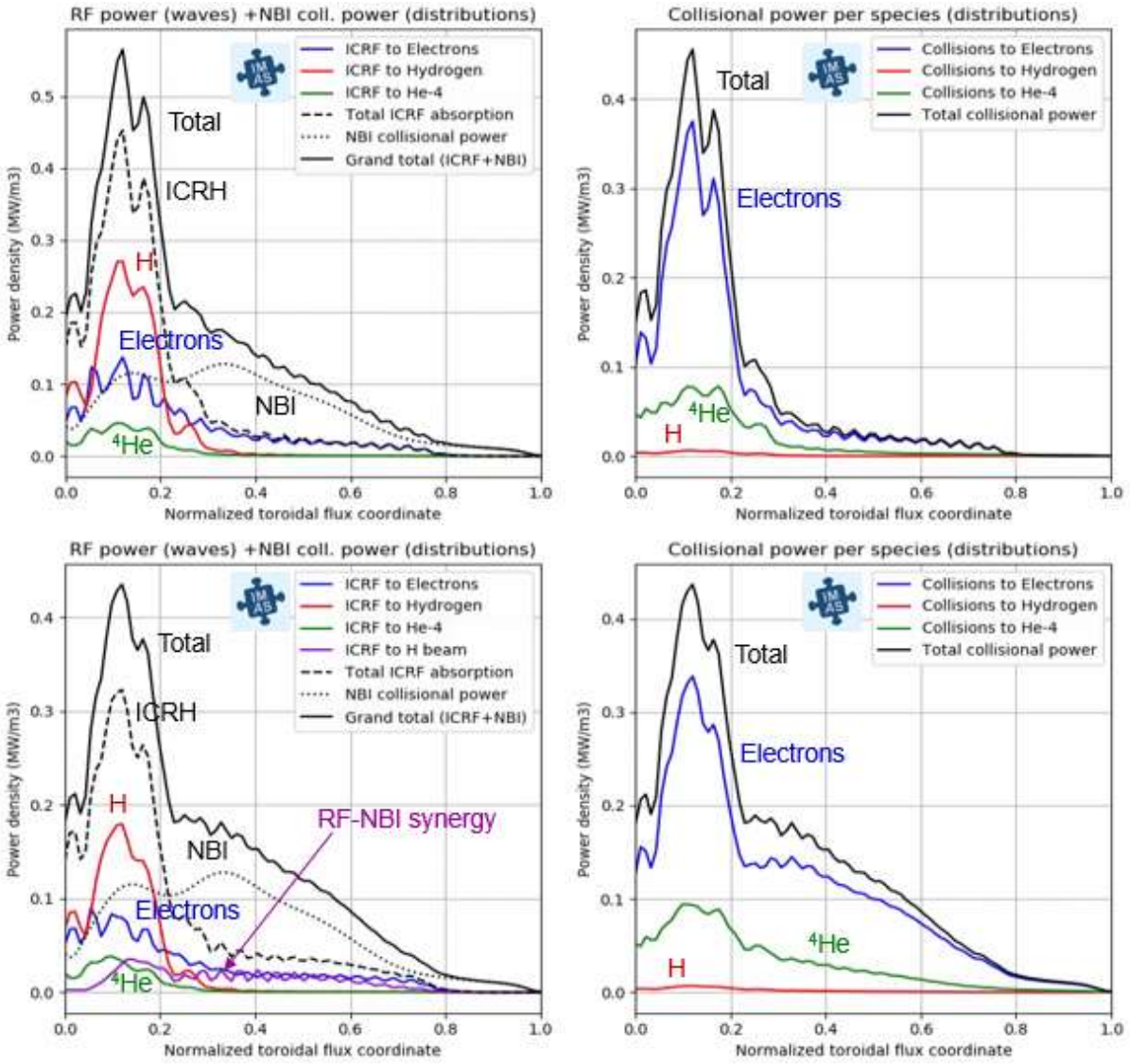

FIG. 9. ICRH absorption and collisional power transfer for an ITER helium H-mode 7.5MA/2.65T scenario. Top figures: with decoupled ICRH and NBI source calculation. Bottom figures: accounting for the NBI+ICRH synergy. Left figures show the IC wave absorption computed by CYRANO along with NBI collisional power density computed by NEMO-RISK. Right figures display the resulting total collisional power computed by FOPLA.

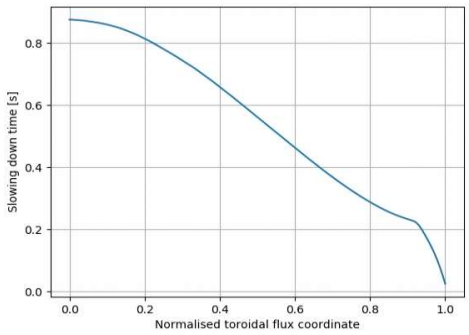

FIG. 10. Hydrogen slowing down time at the flat-top of the JINTRAC H-mode helium scenario at 7.5 MA / 2.65 T.

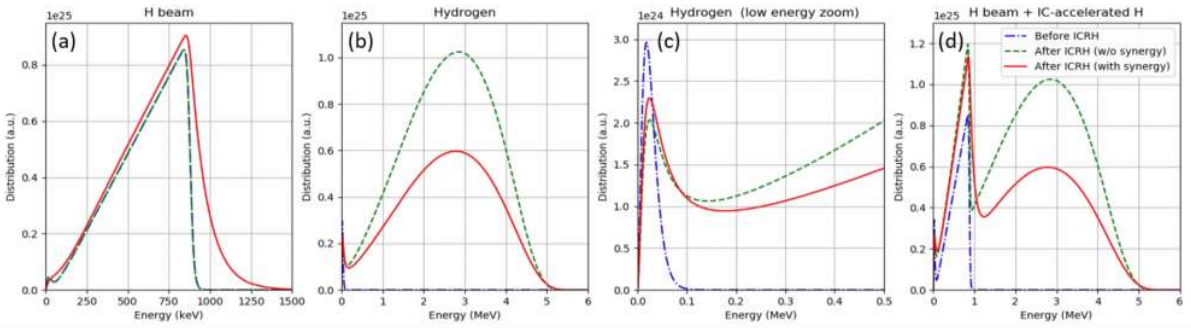

FIG. 11. Energy distributions of H beams and thermal/IC-accelerated H distributions:(a) H beam distribution before and after ICRH (with and without synergy); (b) Distribution of thermal hydrogen (i.e. before ICRH) and IC-accelerated hydrogen (with and without synergy); (c) is the same as (b) but zoomed at low energy; (d) combined distribution of H coming from neutral beams and from initially thermal hydrogen distribution before and after ICRH (with and without synergy).

An interesting aspect to discuss is the effect of the NBI+ICRH synergy on fusion reactions. The fusion reaction cross-section is sensitive to the relative velocity of the interacting species. Synergetic effects occur when the impact of the combination of two heating schemes yields a different result than the summed impact of the two schemes apart. Classically, ICRH+NBI synergy is known to enhance the fusion reaction rate since beam "pre-heating" makes the plasma less collisional and – the steady state reached being a balance between the acceleration by the waves and the deceleration by the collisions – allows higher energy tails to be formed for a given amount of ICRH power. In the present case, the situation is however more subtle: rather than pushing particles into a region where the cross-section is higher, the combined effect of slowing down and wave induced acceleration may result in a decreased fusion rate depending on the birth energy of the beam population, and on the relative strengths of slowing down and acceleration. For the specific example at hand, this is the case: The neutron rate associated with ^{9}Be-p reactions is reduced by an order of magnitude because the wave power is spread over a wider region, yielding lower tail energies and hence less reactions. This effect was already demonstrated in [6] and has recently been confirmed by simulations [30] using the FUSREAC code for calculating nuclear reactions [31,32].

Note that the MeV range H+ ions may have relatively wide orbits so that the zero orbit width approach used in these simulations is not fully accurate and may be overestimating the H+ tails represented in Fig. 11. A 3D Fokker-Planck with the full quasi-linear RF operator (not available yet) would be better suited for a more accurate description of the actual dynamics of the MeV range particles accelerated by ICRH. Note also that the synergetic effect is more prominent if the antenna phasing is optimised for Ion Cyclotron Current Drive (ICCD) when the high energy ion tails are more populated [5].

6. EC ABSORPTION AT 2.65 T IN THE ITER PFPO PHASE

Another application of the H&CD workflow is for the study of EC absorption in the PFPO helium scenario at 7.5 MA / 2.65 T used in Section 5. The Electron Cyclotron Heating for this scenario is based on 2nd harmonic absorption with the X-mode polarization of the wave (X2). Note that for this scenario at low density the pedestal

pressure estimated by the EPED1+SOLPS pedestal model [33] predicts that the pedestal electron temperature is high, i.e. of the order of 3.0-3.5 keV (see Fig. 8), so that for a frequency of 170 GHz and a magnetic field of 2.65 T, the Doppler-shifted 3rd harmonic resonance is located inside the plasma near the edge, leading to a possible X3 parasitic absorption. To simulate the ECH absorption, the TORBEAM and GRAY codes have been applied to this scenario, for an EC power of 20 MW launched from the equatorial launcher with a toroidal angle of 25 degrees (fixed) and a poloidal angle of 0 degrees (steerable), artificially varying the magnetic field (Fig. 12.a) and the wave polarization (Fig. 12.b). For simplicity, the 20 MW are launched from a single mirror of the equatorial launcher, although in practice one single mirror can receive the power from only 8 gyrotrons, i.e. ~6.7 MW. As can be seen, at 2.65 T the ECH absorption is significant at the edge, due to the X3 resonance. It is found that the parasitic edge X3 absorption does not change significantly when varying the poloidal steering angle from 0 to 35 degrees.

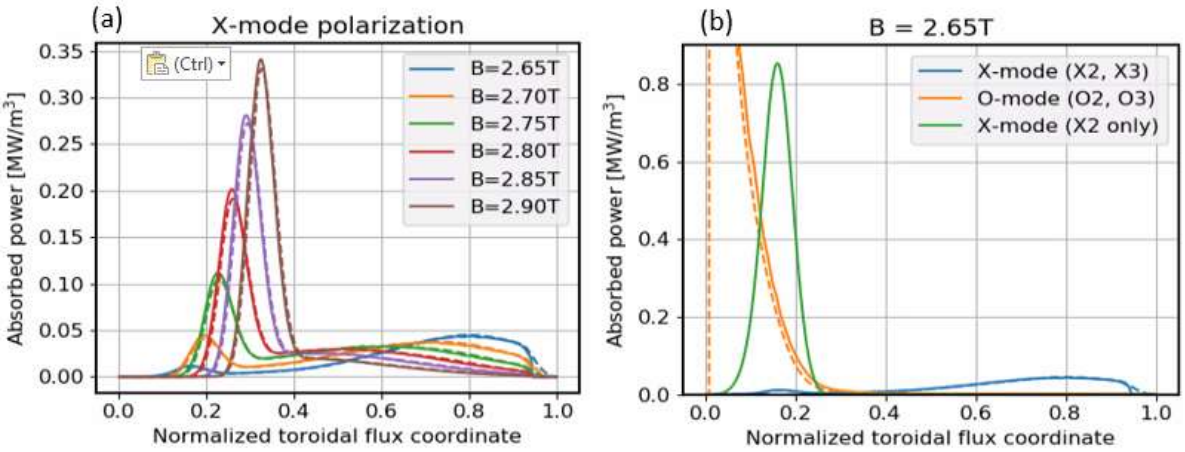

FIG. 12. ECH absorption profiles for an ITER helium H-mode 7.5 MA / 2.65 T scenario: (a) ECH absorption for an X-mode polarization at various values of the magnetic field; (b) ECH absorption at 2.65 T for X-mode (including both X2 and X3 resonances, and with X2 resonance only) and O-mode polarizations. Solid and dashed lines come from TORBEAM and GRAY simulations respectively.

Excellent agreement is found between the TORBEAM and GRAY codes. Note that switching from a code to another is straightforward using the GUI of the H&CD workflow (see Fig. 3), which shows how modular the IMAS environment is and how suitable it is for benchmark activities, given that the standardized data approach ensures identical input for all implemented codes. The results in Fig. 12.a show that when the magnetic field is increased, the edge absorption decreases as the X3 resonance layer moves out of the plasma and the central absorption increases since the X2 absorption becomes more dominant. However, at higher field the X2 absorption is less central and this is less optimal for e.g. central impurity accumulation avoidance. The fraction of EC power absorbed by the X2 and X3 resonances is displayed in Fig. 13 showing that the fraction of X2 absorption increases when the magnetic field is raised.

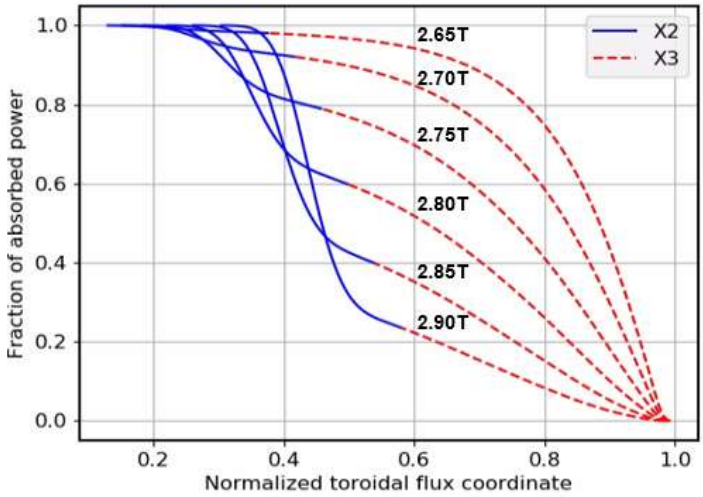

FIG. 13. Fraction of EC power absorbed by X2 and X3 resonances for various values of the magnetic field. The scan is based on an ITER helium H-mode 7.5MA/2.65T scenario.

This observation of strong and undesirable peripheral X3 absorption suggests that an option to avoid it is to increase the magnetic field by a few percent in order to remove it. However this option also leads to a less central X2 ECH absorption and to an increase of the L-H power threshold ($P_{L-H} \sim B^{0.8}$, see [34]). An alternative approach is to change the polarization to O-mode, as shown in Fig. 12.b, leading to a central O2 absorption, since the O3 absorption mechanism is very weak. However the O2 absorption is usually avoided in ITER plasmas because it generates less ECCD than the X2 one, and it also induces significant shine-through power fluxes due to partial absorption for a large range of poloidal steering angles, which can limit the applications of the EC system for current profile tailoring or NTM control.

To quantify these effects, we have modelled the O-mode current density profiles and those for X-mode for various values of the magnetic field. In Fig. 14.a., ECCD profiles for X-mode are shown and the comparison of ECCD profiles between X-mode ignoring the X3 absorption (best case scenario), X-mode including X3 absorption (realistic scenario) and O-mode is displayed in Fig. 14.b. Total ECCD values for all these cases are shown in Table 2. Note that with the convention of the IMAS coordinate system, negative ECCD values mean co-current injection. As can be seen, the total ECCD is 0.6 MA for X2 absorption without X3 resonance, which is reduced to 0.5 MA when switching to O-mode: it confirms that O-mode generates less ECCD than X-mode. However the X2 evaluation does not account for 3rd harmonic absorption; when the X3 resonance is included, the ECCD for X2 (+X3) drops to 29 kA, in which case O-mode becomes much more favourable than X2.

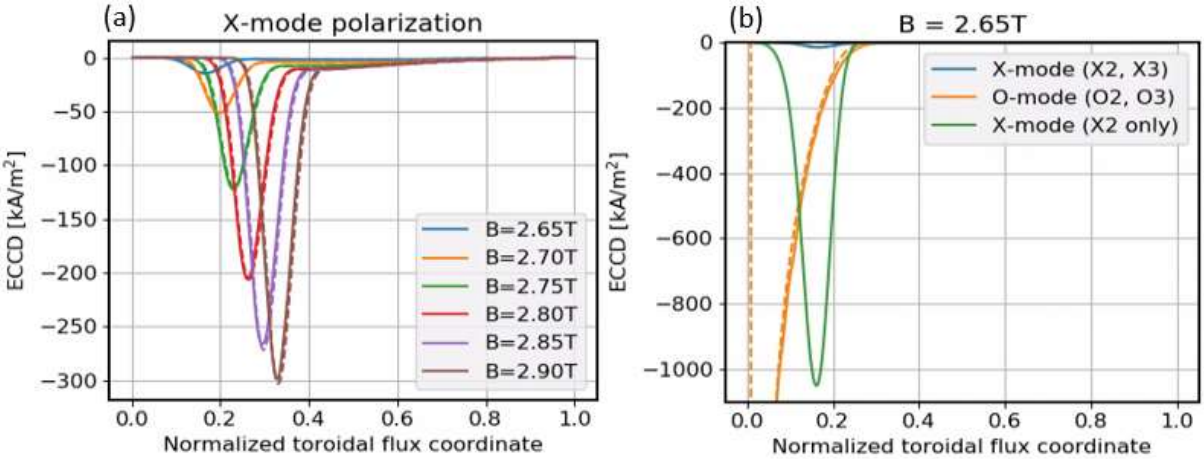

FIG. 14. ECCD profiles for an ITER helium H-mode 7.5MA/2.65T scenario: (a) ECCD for an X-mode polarization at various values of the magnetic field; (b) ECCD absorption at 2.65 T for X-mode (including both X2 and X3 resonances, and with X2 resonance only) and O-mode polarizations. Solid and dashed lines come from TORBEAM and GRAY simulations respectively.

TABLE 2. Integrated ECCD values calculated by TORBEAM and GRAY wave codes, for an ITER helium H-mode 7.5MA/2.65T scenario, for an X-mode polarization at various values of the magnetic field, and at 2.65 T for X-mode (including both X2 and X3 resonances, and with X2 resonance only) and O-mode polarizations.

Polarisation and harmonics	**B-field (T)**	**ECCD (MA) TORBEAM**	**ECCD (MA) GRAY**
X-mode (including X2 and X3)	**2.65**	-0.029	-0.027
	2.70	-0.082	-0.076
	2.75	-0.169	-0.160
	2.80	-0.268	-0.258
	2.85	-0.347	-0.336
	2.90	-0.387	-0.377
X-mode (X2 only)	**2.65**	-0.592	-*
O-mode (O2, O3)	**2.65**	-0.501	-0.511

* *The X2 resonance only case is shown only with TORBEAM since GRAY has no option to remove it from the calculation.*

However, as mentioned earlier, O2 absorption may induce significant shine-through power fluxes due to partial absorption losses for a large range of poloidal steering angles. The absorbed power has been evaluated for these cases in Table 3, which shows the total EC absorbed power in X-mode and O-mode for a large range of poloidal steering angles.

In ITER stationary conditions, the design stationary power handling capability on the beryllium first wall is 2 MW/m2 on normal heat flux panels and 4.7 MW/m2 on enhanced heat flux panels. Thermal loads on the first wall come from plasma thermal fluxes, photonic charge exchange fluxes, EC stray radiation, NBI shine-through, fast particle losses (NBI, ICRH and alpha particles), IC rectified sheaths, etc. All these processes do not necessarily cause power fluxes at the same locations on the first wall. To remain within limits compatible with first wall power fluxes in ITER full field and half field scenarios, the phase with low EC absorption shall be limited to at most 5 seconds while in stationary conditions the EC absorption should be at least 95% due to direct deposition of the non-absorbed beam on the first wall. This accounts for the possible fraction of the beam injected with the wrong polarization (up to 5%), leading to strong refraction and/or reflection at the cut-off layer [35].

The values in Table 3 suggest that in X-mode the poloidal steering angle can be varied from 0 to 30 degrees, keeping almost 100% of absorbed power. However in O-mode, the range of accessible poloidal angles, to keep the shine-through losses within reasonable limits, is reduced to [0-10] degrees, which gives less operational flexibility for the EC system.

The ECH absorption profiles for the various values of the poloidal angles in the case of O-mode polarization are shown in Fig. 15. They show that limiting the steering range of the poloidal angles to [0-10] degrees corresponds to limiting the ECH location from the equatorial launcher to [0;0.2] of the normalized toroidal flux coordinate. This can be a constraint when the EC system is used e.g. for sawtooth control in case e.g. of non-classical non-linear behaviour near the q=1 surface, or for ECCD optimization and current profile shaping which will also be studied during the PFPO phase. Furthermore, the ECH/ECCD location can also modify the density profile pump-out and toroidal rotation, depending on how on or off-axis the deposition is. These are also effects to be studied in ITER PFPO phases.

TABLE 3. Integrated EC absorption values calculated by TORBEAM and GRAY wave codes, for an ITER helium H-mode 7.5 MA/2.65 T scenario, for X-mode and O-mode polarizations at various values of poloidal angles.

Polarisation	**α (degrees)**	**P_{ABS} (MW) TORBEAM**	**P_{ABS} (MW) GRAY**
X-mode	**0**	20	20
	5	20	20
	10	20	20
	15	20	20
	20	20	20
	25	20	20
	30	19.9	20
	35	12.0	12.2
O-mode	**0**	19.3	19.3
	5	18.8	18.8
	10	17.8	17.9
	15	16.4	16.5
	20	14.8	15.1
	25	13.2	13.6
	30	9.55	11.4
	35	1.36	4.29

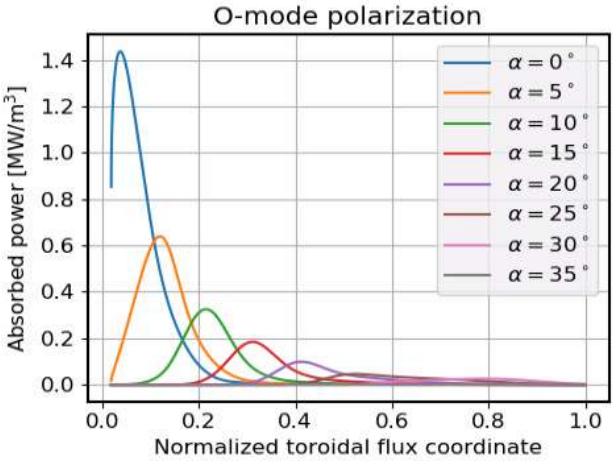

FIG. 15. ECH profiles evaluated by the TORBEAM code for an ITER helium H-mode 7.5 MA / 2.65 T scenario, for various values of poloidal angle of the EC equatorial launcher.

These results have been obtained using a 7.5 MA / 2.65 T H-mode scenario, which represents the worst conditions in terms of X3 edge parasitic absorption, due to the high pedestal leading to large edge values of temperature and density, as seen in Fig. 8. For this reason, it is useful to also study an L-mode case to quantify the X3 parasitic absorption when the pedestal is not formed yet. The temperature and density profiles for an L-mode 7.5 MA / 2.65 T scenario, here computed with the METIS transport solver, applying 20 MW of ECH and 10 MW of ICRH, are displayed in Fig. 16. The resulting ECH and ECCD profiles for a scan of poloidal steering angles, in X-mode, are displayed in Fig. 17. As can be seen, this scenario does not suffer from X3 edge parasitic absorption, except for the extreme value of a poloidal angle of 35 degrees. This means that X-mode operation does not present major issue when injecting EC power in an L-mode plasma. Hence, issues would arise during the L-H transition when the pedestal builds up. For this reason, changing the EC polarization in real time from X- to O-mode during an L-H transition is foreseen, to avoid the appearance of the X3 edge absorption during the formation of the pedestal, which can be done within three seconds with the ITER EC system. This process requires a fast and accurate detection of the L-H transition using the instrumentation available in the PFPO phases, which is the topic of parallel studies [36]. Modelling such dynamic processes needs self-consistent simulations between H&CD and transport. This illustrates how crucial it is to couple H&CD calculations with transport solvers, which was the underlying motivation of integrating the H&CD workflow within the JINTRAC transport suite. It ensures self-consistent modelling of H&CD sources on the plasma transport timescales to follow the dynamics of the discharge, which is one major goal of the IMAS High Fidelity Plasma Simulator currently under development.

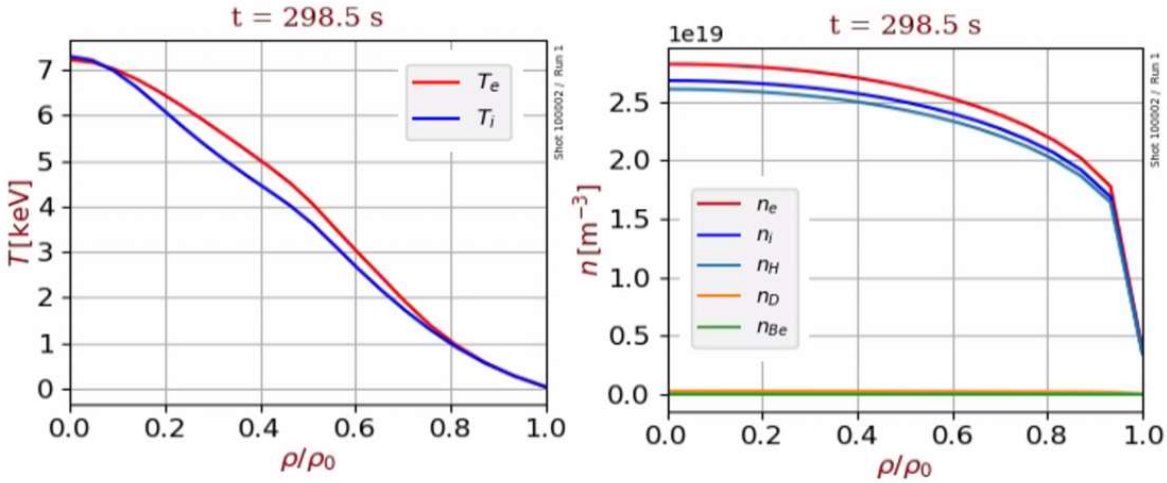

FIG. 16. Temperature and density profiles at the flat-top of a METIS L-mode scenario simulation at 7.5 MA / 2.65 T in hydrogen, including 20 MW of ECH and 10 MW of ICRH.

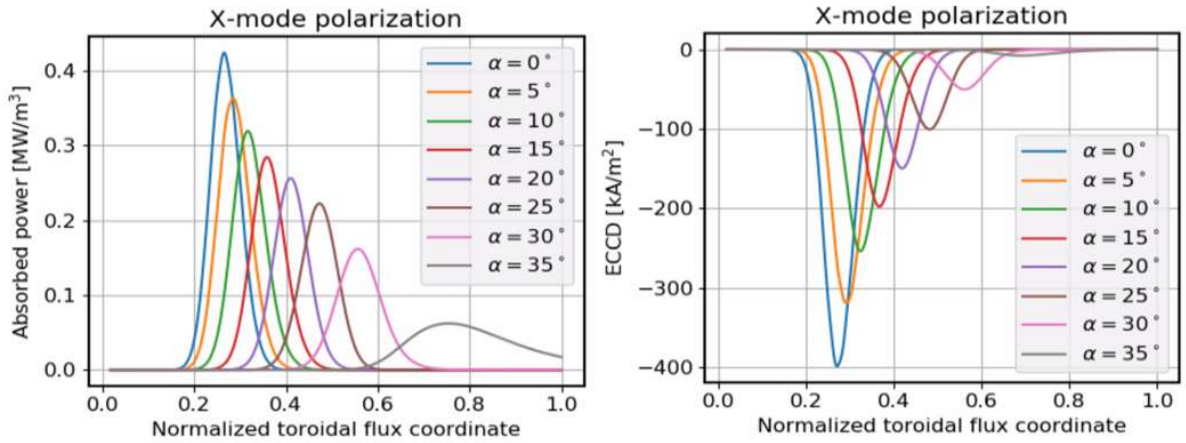

FIG. 17. ECH and ECCD profiles evaluated by the GRAY code for an ITER hydrogen L-mode 7.5 MA / 2.65 T scenario simulation for various values of poloidal angle of the launcher.

7. CONCLUSION

The H&CD workflow has been developed as a key component of the IMAS High Fidelity Plasma Simulator. It offers a high degree of modularity as a workflow component but also for the choice of its intrinsic physics models. Its internal structure has been generalised to enable any kind of algorithm implementation for dedicated physics studies, allowing full flexibility for modelling H&CD processes.

One example of physics studies performed with this H&CD workflow is an examination of the synergetic effects between NBI ions, fusion-born alpha particles and IC waves in ITER DT scenarios. It has been shown that for a 15 MA / 5.3 T baseline DT scenario, applying 33 MW NBI deuterium beams and 10 MW of ICRH tuned at 40 MHz for a central fundamental D heating, the synergetic effects are modest (below 5%), while the RF-NBI synergy is more significant in helium plasmas of the ITER PFPO-2 phase with hydrogen beams combined with fundamental hydrogen heating. For this scenario, the synergetic effects lead to a reduction of the neutron rate by one order of magnitude due to the increased width of the wave power deposition profile on NBI ions which causes a reduction of the local IC power density, yielding a smaller number of fast protons with energies above the threshold of the fusion reactions.

ECH absorption has also been studied in a PFPO 7.5 MA / 2.65 T H-mode scenario, showing a possible issue with parasitic X3 absorption at the plasma edge which can be avoided by slightly increasing the magnetic field or switching to O-mode polarization. Both options have consequences on the overall performance of the EC system, but complications can be avoided by changing the wave polarization in real time from X- to O-mode during the L-H transition.

The present analyses show the capabilities and strengths of the H&CD workflow and its components to simulate the combined effects of NBI, fusion-born alpha particles, ICRH and ECH, essential to accurately predict the performance of ITER plasmas for the various scenarios of the Research Plan. The next step will be to further exploit the H&CD workflow inside the JINTRAC transport solver to model further scenarios of the ITER Research Plan. JINTRAC is itself being coupled to the DINA free boundary equilibrium code, to build the High-Fidelity Plasma Simulator which will become the reference for future predictions of ITER scenarios, and later for supporting ITER operation.

ACKNOWLEDGEMENTS

ITER is a Nuclear Facility INB-174. The views and opinions expressed herein do not necessarily reflect those of the ITER Organization. This work has been supported by the ITER Scientist Fellow Network.

REFERENCES

[1] F. Imbeaux et al, *Nucl. Fusion* **55** (2015) 123006

[2] G. Falchetto et al., *Nucl. Fusion* **54** (2014), 043018

[3] G. Falchetto et al, *26th IAEA Fusion Energy Conference*, Kyoto, Japan (2016), TH-P2-13

[4] ITER Research Plan, ITER Technical Report ITR-18-03
[5] R. Bilato et al, "Synergies between H-NBI fast-ions and ICRF heating in the non-activated operational phase of ITER", 45th EPS Conf. on Plasma Physics (Prague, Czech Republic, July 2–6, 2018)
[6] A.R. Polevoi et al, *Nucl. Fusion* **61** 076008 (2021)
[7] M. Romanelli et al, *Plasma Fusion Res*. **9** (2014) 3403023
[8] P. Lauber et al, "Energetic Particle dynamics induced by off-axis Neutral Beam Injection on ASDEX Upgrade, JT-60SA and ITER", IAEA Fusion Energy Conference (2021) – IAEA TH/P1-20
[9] A.P. Smirnov and R.W Harvey (2003) Technical Report CompX-2000-01 Ver. 2
[10] D. Farina, *Fusion Sci. Technol.* **52** (2007) 154
[11] F. Köchl, scaling based on C. Zucca et al, AIP Conf. Proc. 1069, 361 (2008)
[12] E. Poli et al, Comp. Physics Comm. **225** (2018) 36–46
[13] P. U. Lamalle, "*Nonlocal theoretical generalisation and tridimensional study of the coupling of an ICRH antenna to a tokamak plasma*", Ph.D. thesis, LPP-ERM/KMS report 101, Université de Mons, 1994
[14] L. Villard et al *Comput. Phys. Rep.* **4** (1986) 95
[15] L.-G. Eriksson al, *Nucl. Fusion* **33** (1993) 1037
[16] D. Van Eester and R. Koch, *Plasma Phys. Control. Fusion* **40** (1998) 1949–1975
[17] E. Hirvijoki et al, *Comp. Phys. Comm.,* **185(4)** (2014) 1310
[18] D. Van Eester et al, J. Plasma Phys. (2021), vol. 87, 855870202
[19] M. Schneider et al, *Plasma Phys. Control. Fusion* **47** (2005) 2087–2106
[20] D. Van Eester and E. Lerche, *Plasma Phys. Control. Fusion* **53** (2011) 092001
[21] O. Asunta et al, *Comp. Phys. Comm.* **188** (2015) 33-46
[22] M. Schneider et al, *Nucl. Fusion* **51** (2011) 063019
[23] M. Schneider et al, *Nucl. Fusion* **55** (2015) 013003
[24] P. Sirén et al, *Nucl. Fusion* **58** (2018) 016023
[25] J.F. Artaud et al, *Nucl. Fusion* **58** (2018) 10500
[26] S.D. Pinches et al, "Integrated Modelling & Analysis Suite: developments to address ITER needs", IAEA Fusion Energy Conference (2021) – IAEA-TH/P2-22
[27] E Lerche et al 2009 *Plasma Phys. Control. Fusion* **51** 044006
[28] A V Krasilnikov et al 2009 *Plasma Phys. Control. Fusion* **51** 044005
[29] T.H. Stix 1975 Nucl. Fusion 15 737
[30] D. Van Eester and E. Lerche, *Private Communication* (2021)
[31] D. Van Eester et al, *J. Plasma Phys.* (2021), vol. **87**, 855870202
[32] P. Huynh et al, accepted to Nucl. Fusion https://doi.org/10.1088/1741-4326/ac0b34 (2021)
[33] A.R. Polevoi, et.al., Nucl. Fusion **57** (2017) 02201
[34] Y.R. Martin al, *J. Phys.: Conf. Ser.* **123** (2008) 012033
[35] F. Gandini et al, "Stray RF power estimates from EC exploitation during ITER plasma operations", AIP Conference Proceedings 1406, 173 (2011); https://doi.org/10.1063/1.3664955
[36] A. Medvedeva et al, "*Assessment of L-H transition detection in ITER PFPO phases with synthetic diagnostics*", 5th Asia Pacific Conference on Plasma Physics, AAPPS-DPP2021 (2021)